

Numerical Investigation of Energy Absorption Performance in Thin-Walled Structure Under Three-Point Bending Test

Serdar Halis^{1*}  and Murat Altın² 

¹ Automotive Engineering Department, Faculty of Technology, Pamukkale University, Denizli, 20160, Türkiye

² Automotive Engineering Department, Faculty of Technology, Gazi University, Ankara, 06560, Türkiye

Abstract

The components used to absorb and dissipate the effects of the kinetic energy generated during impact are vital for improving the safety standard of vehicles. Among these, the bending behavior of thin-walled beams in particular plays a critical role in effectively managing the effects of the forces generated in a crash. Furthermore, the material selection of these beams helps to maximize the safety of the occupants inside the vehicle by increasing structural durability. Therefore, the correct positioning and engineering appropriate design of such components in vehicle design is a critical factor to minimize damage from accidents and ensure the safety of occupants. The effective use of these components increases overall vehicle safety by ensuring that vehicles pass crash tests successfully and meet industry standards. In this study, thin-walled beams with seven different geometric structures were designed using the finite element method. In addition, the energy absorption capacities of these designs for three different materials are investigated by considering two important parameters such as specific energy absorption (SEA) and crush force efficiency (CFE). The highest values of both CFE and SEA parameters for the best performing model were obtained with E-glass/PET199 composite material. The use of E-glass/PET199 composite material provided an improvement of 2.32% in the CFE value, while the SEA value remained at the same level (1.08 kJ/kg) as the AA6063-T1 material.

Keywords: Finite element analysis; Crush force efficiency (CFE); Specific energy absorption (SEA); Thin-walled structures; Three-point bending.

Research Article

History

Received 09.02.2024
Revised 02.03.2024
Accepted 19.03.2024

Contact

* Corresponding author
Serdar Halis
shalis@pau.edu.tr
Address: Automotive
Engineering Department,
Faculty of Technology,
Pamukkale University,
Denizli, Türkiye
Tel: +90 258 296 4116

To cite this paper: Halis, S., Altın, M. Numerical Investigation of Energy Absorption Performance in Thin-Walled Structure Under Three-Point Bending Test. International Journal of Automotive Science and Technology. 2024; 8 (1): 159-166. <http://dx.doi.org/10.29228/ijastech..1434645>

1. Introduction

The automotive industry is a sector that is developing continuously in order to increase driver and passenger safety and driving comfort [1,2]. Energy absorbing components play a more critical role when passenger and vehicle safety is taken into account, especially in the automotive sector. Energy absorbers in the vehicle chassis absorb energy by plastic deformation during a crash, thus diminishing the axial force transmitted to the passenger compartment and contributing to passenger safety [3,4]. The most widely used of these energy absorber components are thin-walled structures [5-7] and thin-walled structures filled with cellular materials such as foams or honeycombs [8-11]. While calculating the energy absorption capacity of multicellular and thin-walled structures with different sections, mechanical behaviors such as bending [13-17] and torsion [18,19] are considered. Recently, experimental and numerical studies have been carried out to investigate and improve the mechanical behavior of these structures. Especially three-point bending test is used to evaluate

the bending behavior of thin-walled structures with rectangular and circular sections against an applied force. This test is preferred to obtain mechanical behaviors such as bending strength, the determination of the elastic modulus and the fracture strength of the material. A study in which various theoretical models were proposed to obtain the bending moment at the cross-sectional center of a structure under three-point bending test in accordance with the deformation modes, the validation of the theoretical models was confirmed by using a numerical model that was validated by three-point bending tests [20]. Huang and Zhang [21] proposed a theoretical method to predict the properties of rectangular thin-walled structures based on three-point bending test. The results show that the proposed method has a good prediction of the bending properties of rectangular thin-walled structures. In another study, a hybrid model (Al/CFRP) for a beam structure using aluminum (Al) and carbon fiber reinforced plastic (CFRP) materials was introduced. Three-point bending tests were conducted and a finite element model (FEM) was used to

investigate the quasi-static and dynamic bending properties and energy dissipation of these structures. As a result of this study, it was stated that a 70.6% improvement of specific energy absorption (SEA) was obtained with the Al/CFRP model [22]. An experimental study by Kim et al. [23] examined the quasi-static collapse of Al/CFRP beams, and they found that CFRP wrapping improved Al profile energy absorption by 30%. Sun et al. [24] investigated the bending response of Al/CFRP hybrid structures under quasi-static loads and reported a 43% improvement in SEA with proper CFRP orientation. They stated that under dynamic loading conditions, the composite beams' bending response is significantly more complicated since different deformation properties and collapse mechanisms can result from the combined impacts of strain rate and inertia. Huang et al. [25,26] evaluated a hybrid Al/CFRP structure's transverse bend during static and dynamic loading. They determined that the fibers fractured earlier and also that the bending deformation of double-cell hybrid beams was induced under dynamic loading. Abdullahi and Gao [27] proposed novel different types of cell structures with random cell sizes to provide more energy absorption than conventional square tube structures using the random distribution structure of Voronoi tessellations. These structures were numerically analyzed exposed to axial and bending loads using a FEM, and experiments were conducted for validation of these results. They reported that the suggested multi-cell structures have a higher peak crushing force (PCF) while better SEA values are obtained with regular multi-cell square structures under lateral bending load. Wang et al. [28] researched the resistance of multicellular square tubes to three-point bending test. They performed the bending test using a nonlinear finite element model and conducted experimental test studies to validate the numerical model. According to the test studies, they observed that the number of partition plates significantly affects the structure's bending resistance and the change of load position, which significantly impacts the performance of energy absorption, increases the SEA value by more than 50%.

In this study, seven different thin-walled beams with unique geometries were designed. The materials of the beams were determined as AA6063-T1, mild steel and E-glass/PET199 composite. Each of these designed geometries was subjected to finite element analysis under the same boundary conditions and their energy absorption performances were investigated.

2. Thin-walled beams design concept

In the scope of the study, seven different structures of thin-walled beam tubes were designed. The lengths and wall thicknesses of each structure were taken equal. As a result of the analysis, different names were given to the profiles in order to better specify the results. These models with different unique geometries can be used in many parts of automobiles. For example, they are used in the front and rear parts of the chassis where the crash boxes are connected and in the pillars between the side doors as shown in Figure 1. Figure 2 presents the profiles and the

abbreviated names given to these profiles.

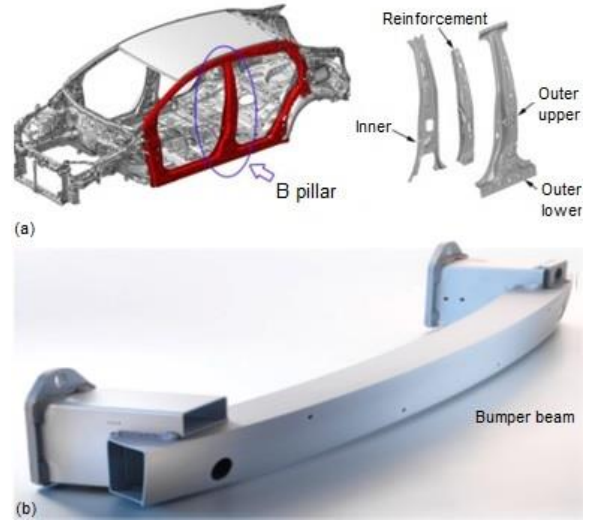


Fig. 1. (a) B pillar and (b) bumper beam structures [29,30].

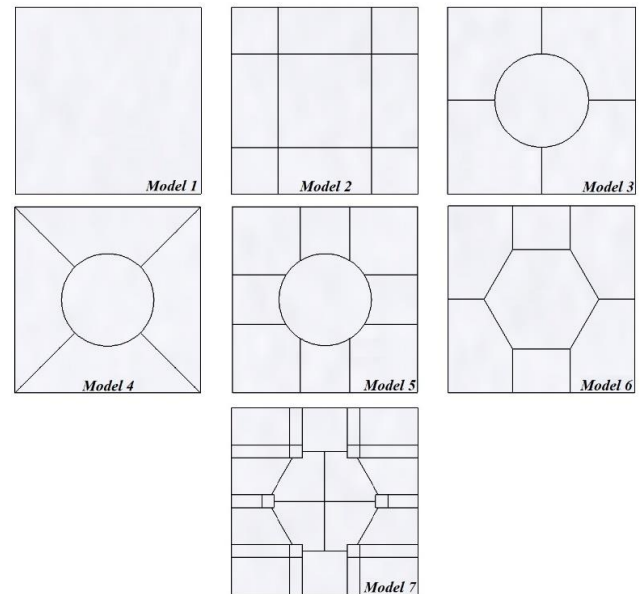


Fig. 2. Cell structures of the thin-walled beams used in the analyses.

3. Finite element modeling

In this part of the study, finite element models of the designed thin-walled beam profiles were created and analyzed. However, before proceeding with the analysis, a validation study was carried out to ensure the accuracy of the setup. The article by Zhang and Fu [20] was used for the validation study. In the article, a three-point bending test was performed experimentally on the test setup in Figure 3, which was prepared according to ASTM E8M-04 test standards for an aluminum profile with a wall thickness of 1.05 mm and a length of 370 mm, consisting of AA6063-T1 material, whose mechanical properties are given in Table 1, and its energy

absorption performance was investigated.

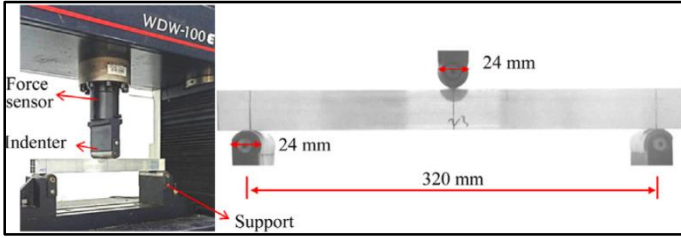


Fig. 3. Configuration for the three-point bending test.

Table 1. The properties of AA6063-T1 [20]

| | |
|-----------------------------|------------------------|
| Density, ρ | 2700 kg/m ³ |
| Poisson's ratio, ν | 0.33 |
| Young's modulus, E | 68.9 GPa |
| Ultimate stress, σ_u | 222.0 MPa |
| Yield stress, σ_y | 100.0 MPa |

Zhang and Fu also validated this experimental study by using the finite element method. In this paper, a validation study was carried out by considering the same boundary conditions before proceeding to the analysis of the specific designs. Hypermesh program was used to form the finite element model of the profile. The finite element model is given in Figure 4.

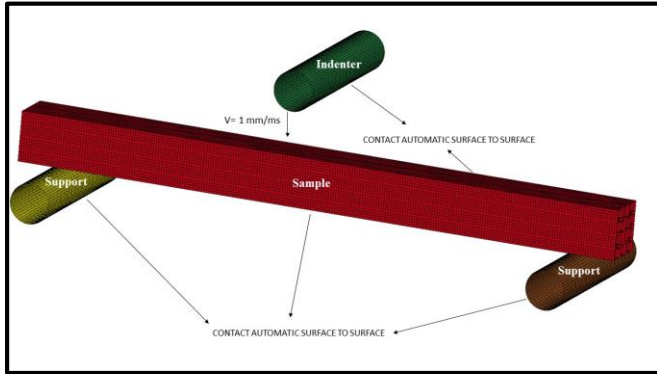


Fig. 4. Finite element model for three-point bending test.

AA6063-T1 material properties are defined in *MAT 24 PIECEWISE LINEAR PLASTICITY* material card via the program. Indenters and supports were modeled as rigid bodies with *MAT_20_RIGID* card. Material fracture was not simulated as no fracture occurred in the samples. Belytschko-Tsay shell elements with two integral points across the thickness direction were used to differentiate the beams, indenters and supports. The contact between beams and rigid indenters or supports is described using the *CONTACT AUTOMATIC SURFACE TO SURFACE* contact card. Possible contact between the inner and outer shell structures with different wall thicknesses of the relevant profile was defined by using the *CONTACT AUTOMATIC SINGLE SURFACE* contact card. While the analysis model was created, the static and

dynamic friction coefficient was assumed to be 0.3 at all interfaces based on the measurements made by Zhang and Fu with the friction angle method. Finally, the prepared models were analyzed with the Ls-Dyna program with a deformation rate of 1 mm/ms. As a result of the analysis, the deformation image was obtained as shown in Figure 5.

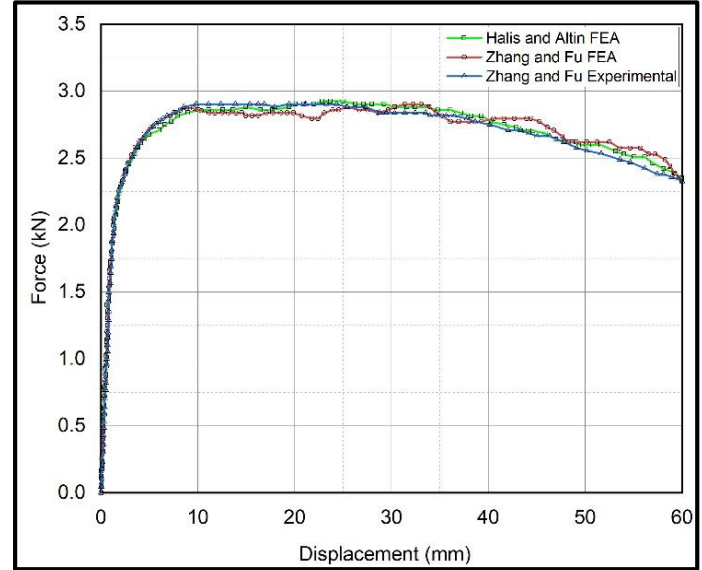


Fig. 5. Deformation of multi-cell sections and force-displacement curves under three-point bending.

In order to describe the results of the analysis numerically, the following metrics are needed.

Total absorbed energy (E_T): It is the total amount of energy absorbed by the energy absorbing profiles as a result of their deformation [7] and is calculated by the formula given in Eq.(1), where F is the crush force in the axial direction and δ is the deformation distance of the energy absorbing structure.

$$E_T = \int_0^{\delta_{max}} F d\delta \quad (1)$$

Average Crush Force (F_{avg}): It is defined as the ratio of the total absorbed energy to the maximum displacement (Eq. 2) [7].

$$F_{avg} = \frac{E_T}{\delta_{max}} \quad (2)$$

Crush Force Efficiency (CFE): As given in Eq. (3), it is the ratio of the average crush force to the maximum crush force (F_{max}) [7]. The maximum crush force is the highest force occurring during deformation of the profiles. This value is expected to be as high as possible for an energy absorber. A high crush force efficiency indicates that the energy absorber has a good efficiency.

$$CFE = \frac{F_{avg}}{F_{max}} \quad (3)$$

Specific Energy Absorption (SEA): This parameter is defined as the amount of energy per unit mass and is calculated by the formula

given in Eq.(4), where m_T is the total mass [7].

$$SEA = \frac{E_T}{m_T} \quad (4)$$

The calculations using these metrics obtained the results given in Table 2. These results show that the validation study was successfully carried out with a quite low percentage of error.

Table 2. The results obtained by calculations

| | Displacement (mm) | Mass (kg) | E_T (kJ) | SEA (kJ/kg) | SEA Error (%) |
|-----------------------|-------------------|-----------|------------|-------------|---------------|
| Zhang and Fu (Test) | 60 | 0,18304 | 0,16184 | 0,88417 | - |
| Zhang and Fu (FEA) | 60 | 0,18304 | 0,16184 | 0,88887 | 0,54 |
| Halis and Altin (FEA) | 60 | 0,18304 | 0,16184 | 0,88882 | 0,53 |

All the operations performed from the beginning to the end of the study are detailed in the flowchart in Figure 6.

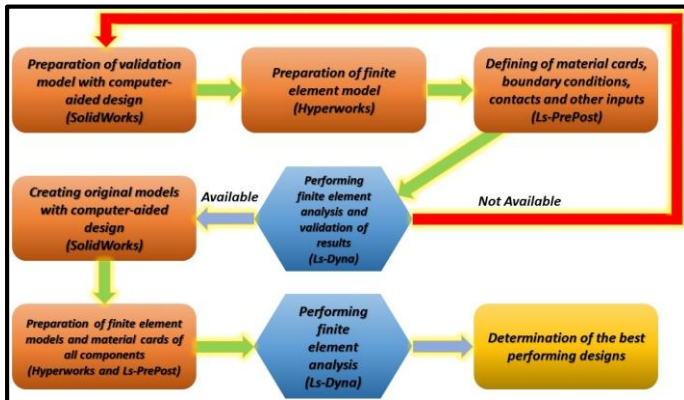


Fig. 6. Flowchart of the FEM for three-point bending test

4. Results and Discussion

In the last part of the study, seven different geometric designs with the original structure given in Figure 1 were analyzed. When the structures were modeled, the wall thickness was 1 mm for each sample. Since the study was parametric, the profiles consisted of three different materials, AA6063-T1 [20], mild steel [31] and E-glass/PET199 composite [32]. Table 3 and Table 4 present the mechanical properties of mild steel and E-glass/PET199 composite materials, respectively.

Table 3. The properties of mild steel [31]

| | |
|--------------------------|------------------------|
| Density, ρ | 7850 kg/m ³ |
| Poisson's ratio, ν | 0.33 |
| Young's modulus, E | 210 GPa |
| Yield stress, σ_y | 304.0 MPa |

Table 4. The properties of E-glass/PET199 composite material [32]

| | |
|--|------------------------|
| Density, ρ | 2000 kg/m ³ |
| Modulus in longitudinal (fiber) direction, E_a | 37.9 GPa |
| Modulus in transverse direction, $E_b=E_c$ | 11.5 GPa |
| Shear modulus, G_{12} | 4.5 GPa |
| Major Poisson's ratio, ν_{12} | 0.29 |
| Minor Poisson's ratio, ν_{21} | 0.0811 |
| Longitudinal tensile strength, X_t | 936 MPa |
| Longitudinal compressive strength, X_c | 484 MPa |
| Transverse tensile strength, Y_t | 25.7 MPa |
| Transverse compressive strength, Y_c | 143 MPa |
| Shear strength, S_c | 16.1 MPa |
| Inter-laminar shear strength, S_b | 62.6 MPa |
| Fiber volume fraction, V_f | 70% |

When the composite material card was created, *MAT 54 ENHANCED COMPOSITE DAMAGE* in the Ls-Dyna material library was used, and when the mild steel was defined, *MAT 24 PIECEWISE LINEAR PLASTICITY* material card was used as in aluminum. As a result, analyses were performed separately for each model and the obtained results are given in Table 5-7.

According to the result data in Table 5-7, if the material was chosen as AA6063-T1 and mild steel, it was determined that Model 3 had the highest CFE but Model 7 showed the best energy absorption characteristics. However, when the material of the profiles was chosen as composite, it was seen that Model 7 had the best performance with regard to both CFE and SEA.

Table 5. The analysis results for AA6063-T1

| <i>Material type: AA6063-T1</i> | | | | | | | |
|---------------------------------|---------|---------|-------------|---------|---------|---------|-------------|
| | Model 1 | Model 2 | Model 3 | Model 4 | Model 5 | Model 6 | Model 7 |
| <i>Displacement (mm)</i> | 60 | 60 | 60 | 60 | 60 | 60 | 60 |
| <i>Peak Crush Force (kN)</i> | 1,84 | 5,67 | 3,07 | 3,51 | 4,24 | 3,94 | 8,04 |
| <i>Energy (kJ)</i> | 0,065 | 0,284 | 0,172 | 0,185 | 0,227 | 0,204 | 0,416 |
| <i>Mean Crush Force (kN)</i> | 1,08 | 4,73 | 2,87 | 3,08 | 3,78 | 3,40 | 6,93 |
| <i>CFE</i> | 0,58 | 0,83 | 0,93 | 0,88 | 0,89 | 0,86 | 0,86 |
| <i>Mass (kg)</i> | 0,3843 | 0,3843 | 0,3843 | 0,3843 | 0,3843 | 0,3843 | 0,3843 |
| <i>SEA (kJ/kg)</i> | 0,17 | 0,74 | 0,45 | 0,48 | 0,59 | 0,53 | 1,08 |

Table 6. The analysis results for Mild steel

| <i>Material type: Mild Steel</i> | | | | | | | |
|----------------------------------|---------|---------|-------------|---------|---------|---------|-------------|
| | Model 1 | Model 2 | Model 3 | Model 4 | Model 5 | Model 6 | Model 7 |
| <i>Displacement (mm)</i> | 60 | 60 | 60 | 60 | 60 | 60 | 60 |
| <i>Peak Crush Force (kN)</i> | 3,80 | 9,09 | 5,22 | 6,00 | 7,01 | 6,71 | 12,97 |
| <i>Energy (kJ)</i> | 0,110 | 0,478 | 0,289 | 0,286 | 0,364 | 0,346 | 0,705 |
| <i>Mean Crush Force (kN)</i> | 1,83 | 7,97 | 4,82 | 4,77 | 6,07 | 5,77 | 11,75 |
| <i>CFE</i> | 0,48 | 0,88 | 0,92 | 0,79 | 0,87 | 0,86 | 0,91 |
| <i>Mass (kg)</i> | 1,1147 | 1,1147 | 1,1147 | 1,1147 | 1,1147 | 1,1147 | 1,1147 |
| <i>SEA (kJ/kg)</i> | 0,10 | 0,43 | 0,26 | 0,26 | 0,33 | 0,31 | 0,63 |

Table 7. The analysis results for Composite E-glass/PET199

| <i>Material type: Composite E-glass/PET199</i> | | | | | | | |
|--|---------|---------|---------|---------|---------|---------|-------------|
| | Model 1 | Model 2 | Model 3 | Model 4 | Model 5 | Model 6 | Model 7 |
| <i>Displacement (mm)</i> | 60 | 60 | 60 | 60 | 60 | 60 | 60 |
| <i>Peak Crush Force (kN)</i> | 1,46 | 4,39 | 2,67 | 3,32 | 3,90 | 3,64 | 5,82 |
| <i>Energy (kJ)</i> | 0,040 | 0,170 | 0,103 | 0,102 | 0,164 | 0,133 | 0,308 |
| <i>Mean Crush Force (kN)</i> | 0,67 | 2,83 | 1,72 | 1,70 | 2,73 | 2,22 | 5,13 |
| <i>CFE</i> | 0,46 | 0,65 | 0,64 | 0,51 | 0,70 | 0,61 | 0,88 |
| <i>Mass (kg)</i> | 0,2847 | 0,2847 | 0,2847 | 0,2847 | 0,2847 | 0,2847 | 0,2847 |
| <i>SEA (kJ/kg)</i> | 0,14 | 0,60 | 0,36 | 0,36 | 0,58 | 0,47 | 1,08 |

Thin-walled beams are used in different areas on automobiles. One of these areas is pillars. Pillars are usually designed as hollow geometries [29,33,34] and are geometrically quite similar to the analyzed Model 1. Likewise, the bumpers [35,36], which are located on the front chassis and mounted on the ends of the crash boxes, are usually hollow and also similar to Model 1. When the analysis results of the original designs are evaluated, it is seen that Model 1 has the lowest SEA and CFE values for almost every material. When the data in Tables 5-7 are evaluated, the results show that the best performance is obtained with Model 7. When the CFE and SEA values obtained by using mild steel and E-glass/PET199 materials compared to the AA6063-T1 material used by Zhan and Fu for Model 7 are considered; although 5.81% improvement in CFE value was achieved with mild steel material, there was a 41.6% decrease in SEA amount. The use of E-glass/PET199 composite material resulted in a 2.32% improvement in the CFE value while the SEA value remained at the same level.

If the materials used in the profiles were examined specifically, it was determined that the highest SEA value for AA6063-T1 was obtained with the use of Model 7 and the highest CFE value was obtained with Model 3. Figure 7 shows the deformation results of Model 3 and Model 7 at different times for AA6063-T1 material. The deformations in other profiles and the results of these deformations were not as high as these two models. The same situation encountered for AA6063-T1 material was also observed when the material of the profiles was selected as mild steel (Figure 8). However, the situation was different when the material of the profiles was selected as Composite E-glass/PET199. Model 7, whose deformation results are shown in Figure 9 at different time intervals, was the best performing model in terms of both CFE and SAE.

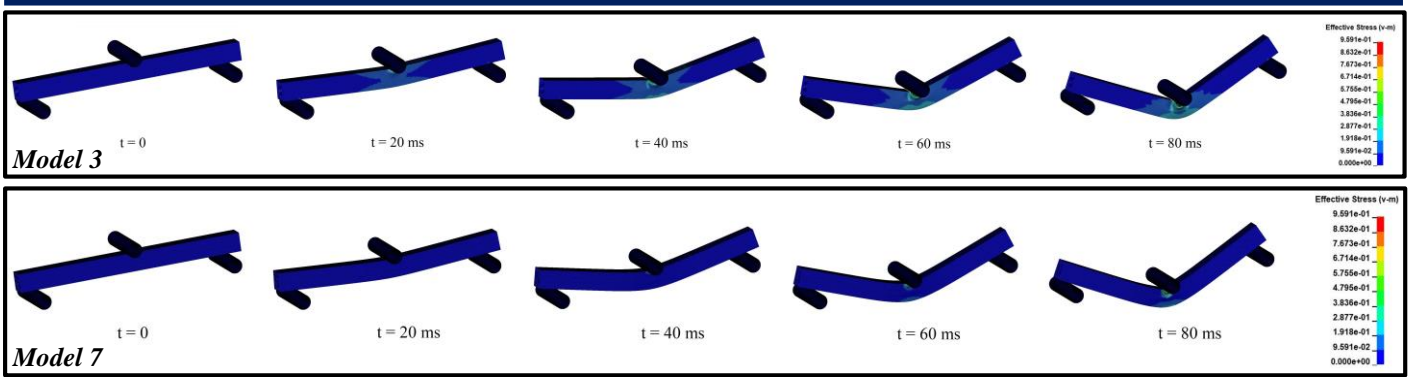


Fig. 7. Deformations of Model 3-7 for AA6063-T1 with FEA in three-point bending test.

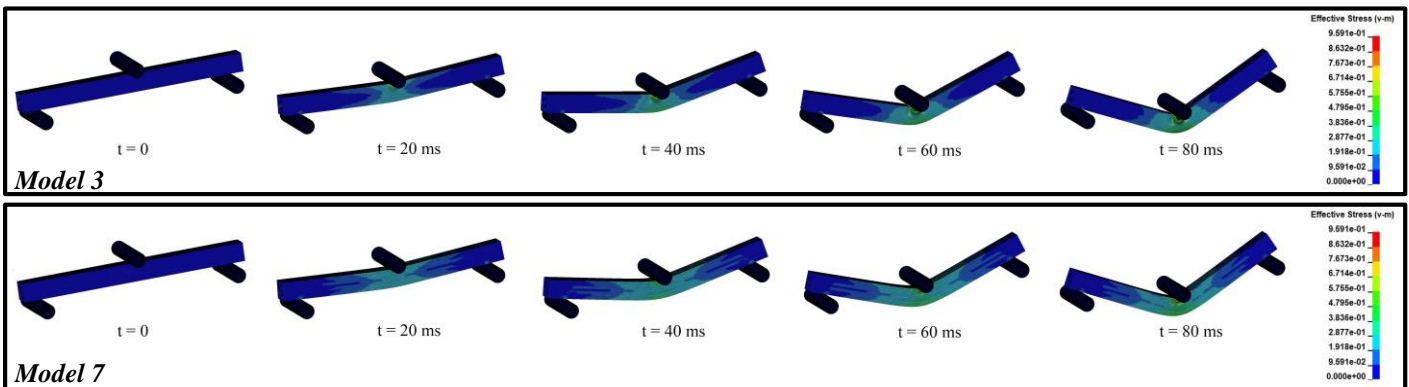


Fig. 8. Deformations of Model 3-7 for Mild Steel with FEA in three-point bending test.

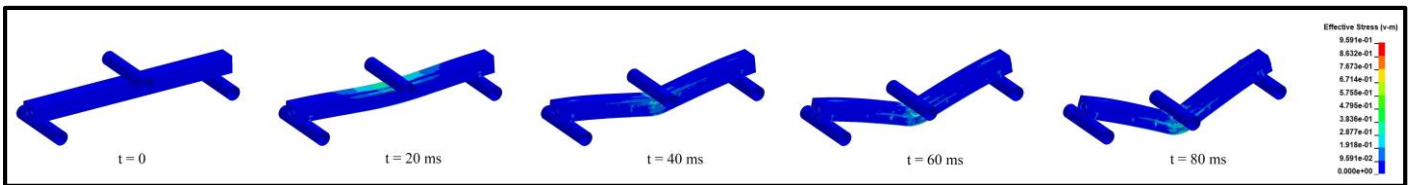


Fig. 9. Deformations of Model 7 for Composite E-glass/PET199 with FEA in three-point bending test.

5. Conclusions

In this research, the energy absorption performance of thin-walled beams of different geometric designs under three-point bending test was investigated using the finite element method. The results obtained are as follows:

- ✚ It was found that Model 7 had the highest SEA value and Model 3 had the highest CFE value for thin-walled beams with AA6063-T1 and mild-steel.
- ✚ The highest SEA and CFE values for thin-walled beams with composite E-glass/PET199 were obtained with model 7.
- ✚ Model 7 was determined to be the best performance thin-walled profile among all designs in general, when all parameters were taken into account.
- ✚ Model 7 was determined to have higher SEA in AA6063-T1 and composite E-glass/PET199 materials and lower SEA in mild steel than Zhang and Fu's models. The lower SEA for mild steel can be explained by the fact that the weight increases at a higher rate than the absorbed energy.

The designed models can be used as alternative designs to conventional front bumpers and pillar used in vehicles. The deformations and crash performances of the models made of AA6063-T1 and Mild steel are similar to each other, but the behavior of the composite E-glass/PET199 material is not similar. The higher crash performance of the composite E-glass/PET199 material is due to its higher resistance to deformation. The conventional designs can be modified in the future and unique profiles can be produced and used in vehicles under real conditions.

Acknowledgment

The authors thank Berat Erbek for his assistance in constructing the preliminary versions of the finite element models.

Conflict of Interest Statement

The authors declare that there is no conflict of interest in the study.

CRediT Author Statement

Serdar Halis: Conceptualization, Writing-original draft, Visualization, Methodology.

Murat Altın: Conceptualization, Data curation, Supervision, Validation.

References

- [1] Arslan TA, Aysal FE, Çelik İ, Bayrakçeken H, Öztürk TN. Quarter car active suspension system control using fuzzy controller. *Engineering Perspective*. 2022;2(4):33-39. <http://dx.doi.org/10.29228/eng.pers.66798>
- [2] Binboğa F, Şimşek HE. Design and optimization of a semi-trailer extendable RUPD according to UNECE R58. *Engineering Perspective*. 2022;2(2):13-20. <http://dx.doi.org/10.29228/eng.pers.62436>
- [3] Josee M, Kazima S, Turabimana P. Review of semi-active suspension based on Magneto-rheological damper. *Engineering Perspective*. 2021;2(2):38-51. <http://dx.doi.org/10.29228/eng.pers.50853>
- [4] Karaman M, Korucu S. Modeling the vehicle movement and braking effect of the hydrostatic regenerative braking system. *Engineering Perspective*. 2023;3(2):18-26. <http://dx.doi.org/10.29228/eng.pers.69826>
- [5] Kocabaş GB, Çetin E, Yalcinkaya S, Şahin Y. Experimental comparison of the energy absorption performance of traditional lattice and novel lattice filled tubes. *International Journal of Automotive Science and Technology*. 2023;7(3):207-212. <https://doi.org/10.30939/ijastech..1331192>
- [6] Kim HS. New extruded multi-cell aluminum profile for maximum crash energy absorption and weight efficiency. *Thin-Walled Structures*. 2002;40(4):311-327. [https://doi.org/10.1016/S0263-8231\(01\)00069-6](https://doi.org/10.1016/S0263-8231(01)00069-6)
- [7] Altın M, Halis S, Yücesu HS. Investigation of the effect of corrugated structure on crashing performance in thin-walled circular tubes. *International Journal of Automotive Science and Technology*. 2017;1(2):1-7.
- [8] Du Z, Duan L, Cheng A, Xu Z, Zhang G. Theoretical prediction and crashworthiness optimization of thin-walled structures with single-box multi-cell section under three-point bending loading. *International Journal of Mechanical Sciences*. 2019;157:703-714. <https://doi.org/10.1016/j.ijmecsci.2019.05.013>
- [9] Zheng D, Zhang J, Lu B, Zhang T. Energy absorption of fully clamped multi-cell square tubes under transverse loading. *Thin-Walled Structures*. 2021;169:108334. <https://doi.org/10.1016/j.tws.2021.108334>
- [10] Zheng G, Wu S, Sun G, Li G, Li Q. Crushing analysis of foam-filled single and bitubal polygonal thin-walled tubes. *International Journal of Mechanical Sciences*. 2014;87:226-240. <https://doi.org/10.1016/j.ijmecsci.2014.06.002>
- [11] Zhang J, Zhou H, Wu L, Chen G. Bending collapse theory of thin-walled twelve right-angle section beams filled with aluminum foam. *Thin-Walled Structures*. 2015;94:45-55. <https://doi.org/10.1016/j.tws.2015.03.024>
- [12] Xiao Z, Fang J, Sun G, Li Q. Crashworthiness design for functionally graded foam-filled bumper beam. *Advances in Engineering Software*. 2015;85:81-95. <https://doi.org/10.1016/j.advengsoft.2015.03.005>
- [13] Kılıçaslan C. Numerical crushing analysis of aluminum foam-filled corrugated single-and double-circular tubes subjected to axial impact loading. *Thin-Walled Structures*. 2015;96:82-94. <https://doi.org/10.1016/j.tws.2015.08.009>
- [14] Zhang J, Wu L, Chen G, Zhou H. Bending collapse theory of thin-walled twelve right-angle section beams. *Thin-Walled Structures*. 2014;85:377-387. <https://doi.org/10.1016/j.tws.2014.09.016>
- [15] Kitarovic S, Zanic V. Approximate approach to progressive collapse analysis of the monotonous thin-walled structures in vertical bending. *Marine Structures*. 2014;39:255-286. <https://doi.org/10.1016/j.marstruc.2014.07.008>
- [16] Gliszczynski A, Czechowski L. Collapse of channel section composite profile subjected to bending. Part I: Numerical investigations. *Composite Structures*. 2017;178:383-394. <https://doi.org/10.1016/j.compstruct.2017.07.033>
- [17] Bai J, Meng G, Wu H, Zuo W. Bending collapse of dual rectangle thin-walled tubes for conceptual design. *Thin-Walled Structures*. 2019;135:185-195. <https://doi.org/10.1016/j.tws.2018.11.014>
- [18] Zaifuddin SAM, Chen DH, Ushijima K. Estimation of maximum torsional moment for multicorner tubes. *Thin-Walled Structures*. 2017;112:66-77. <https://doi.org/10.1016/j.tws.2016.12.005>
- [19] Chen W, Wierzbicki T, Breuer O, Kristiansen K. Torsional crushing of foam-filled thin-walled square columns. *International Journal of Mechanical Sciences*. 2001;43(10):2297-2317. [https://doi.org/10.1016/S0020-7403\(01\)00040-6](https://doi.org/10.1016/S0020-7403(01)00040-6)
- [20] Zhang X, Fu X. New theoretical models for the bending moment of thin-walled beams under three-point bending. *Applied Mathematical Modelling*. 2023;121:21-42. <https://doi.org/10.1016/j.apm.2023.04.015>
- [21] Huang Z, Zhang X. Three-point bending collapse of thin-walled rectangular beams. *International Journal of Mechanical Sciences*. 2018;144:461-479. <https://doi.org/10.1016/j.ijmecsci.2018.06.001>
- [22] Huang Z, Li Y, Zhang X, Chen W, Fang D. A comparative study on the energy absorption mechanism of aluminum/CFRP hybrid beams under quasi-static and dynamic bending. *Thin-Walled Structures*. 2021;163:107772. <https://doi.org/10.1016/j.tws.2021.107772>
- [23] Kim HC, Shin DK, Lee JJ. Characteristics of aluminum/CFRP short square hollow section beam under transverse quasi-static loading. *Composites Part B: Engineering*. 2013;51:345-358. <https://doi.org/10.1016/j.compositesb.2013.03.020>
- [24] Sun G, Pang T, Zheng G, Song J, Li Q. On energy absorption of functionally graded tubes under transverse loading. *International Journal of Mechanical Sciences*. 2016;115:465-480. <https://doi.org/10.1016/j.ijmecsci.2016.06.021>
- [25] Huang Z, Zhang X. Crashworthiness and optimization design of quadruple-cell Aluminum/CFRP hybrid tubes under transverse

- bending. *Composite Structures*. 2020;235:111753.
<https://doi.org/10.1016/j.compstruct.2019.111753>
- [26] Huang Z, Zhang X, Yang C. Experimental and numerical studies on the bending collapse of multi-cell Aluminum/CFRP hybrid tubes. *Composites Part B: Engineering*. 2020;181:107527.
<https://doi.org/10.1016/j.compositesb.2019.107527>
- [27] Abdullahi HS, Gao S. A novel multi-cell square tubal structure based on Voronoi tessellation for enhanced crashworthiness. *Thin-Walled Structures*. 2020;150:106690.
<https://doi.org/10.1016/j.tws.2020.106690>
- [28] Wang Z, Li Z, Zhang X. Bending resistance of thin-walled multi-cell square tubes. *Thin-Walled Structures*. 2016;107:287-299.
<https://doi.org/10.1016/j.tws.2016.06.017>
- [29] Shi D, Watanabe K, Naito J, Funada K, Yasui K. Design optimization and application of hot-stamped B pillar with local patchwork blanks. *Thin-Walled Structures*. 2022;170:108523.
<https://doi.org/10.1016/j.tws.2021.108523>
- [30] Osokoya O. An evaluation of polymer composites for car bumper beam. *International Journal of Automotive Composites*. 2017;3(1):44-60.
<https://doi.org/10.1504/IJAUTO.2017.086521>
- [31] Altin M. Effect of taper angle on crashworthiness performance in hybrid tubes. *International Journal of Automotive Engineering and Technologies*. 2020;9(1):11-19.
<https://doi.org/10.18245/ijaet.638953>
- [32] Zhang Z, Hou S, Liu Q, Han X. Winding orientation optimization design of composite tubes based on quasi-static and dynamic experiments. *Thin-Walled Structures*. 2018;127:425-433.
<https://doi.org/10.1016/j.tws.2017.11.052>
- [33] Sun G, Tian J, Liu T, Yan X, Huang X. Crashworthiness optimization of automotive parts with tailor rolled blank. *Engineering Structures*. 2018;169:201-215.
<https://doi.org/10.1016/j.engstruct.2018.05.050>
- [34] Yu K, Liu Y, Zhang Z. Energy-absorbing analysis and reliability-based multiobjective optimization design of graded thickness B pillar with grey relational analysis. *Thin-Walled Structures*. 2019;145:106364.
<https://doi.org/10.1016/j.tws.2019.106364>
- [35] Marzbanrad J, Alijanpour M, Kiasat MS. Design and analysis of an automotive bumper beam in low-speed frontal crashes. *Thin-Walled Structures*. 2009;47(8-9):902-911.
<https://doi.org/10.1016/j.tws.2009.02.007>
- [36] Wang H, Zhang G, Zhou S, Ouyang L. Implementation of a novel six sigma multi-objective robustness optimization method based on the improved response surface model for bumper system design. *Thin-Walled Structures*. 2021;167:108257.
<https://doi.org/10.1016/j.tws.2021.108257>